CHIN. PHYS. LETT. Vol. 36, No. 5 (2019) 056801

Interplay of Strain and Magnetism in FeSe Monolayers *

Yun Xie(谢云)[1,2], Junsheng Feng(冯俊生)[1,2], Hongjun Xiang(向红军)[1,2], Xingao Gong(龚新高)[1,2**]

[1] *Key Laboratory for Computational Physical Science (Ministry of Education), State Key Laboratory of Surface Physics and Department of Physics, Fudan University, Shanghai 200433*

[2] *Collaborative Innovation Center of Advanced Microstructures, Nanjing University, Nanjing 210093*

(Received 12 March 2019)

Superconductivity and its relationship with strain remains elusive in the monolayer FeSe superconductor. Based on first-principles calculations and model studies, we investigate the magnetic properties of FeSe and FeTe monolayers and find that tensile strain induces changes to magnetic phases for both materials. Furthermore, we reveal that electron doping will decrease the difference of effective magnetic interactions between the a and b directions in an FeSe monolayer and hence suppress its nematicity. We suggest that the overall effect of tensile strain combined with electron doping hinders the appearance of both magnetic and nematic orders in an FeSe monolayer, which paves the way for the emergence of superconductivity.

PACS: 68.35.Gy, 74.70.Xa, 68.43.Bc DOI: 10.1088/0256-307X/36/5/056801

There is no doubt that the substrate plays a significant role in enhancing the T_c of FeSe monolayers.[1−9] For instance, a high-resolution angle-resolved photoemission spectroscopy (ARPES) experiment revealed an unexpected replica band phenomenon that was most probably caused by the coupling between a high-energy optical phonon from the $SrTiO_3$ (STO) substrate and FeSe electrons.[5] Such coupling was believed to raise the superconducting gap opening temperature in FeSe/STO.[1,5,10,11] On the other hand, the superconducting phase of monolayer FeSe only emerges when doped by substantial electron donation from the STO substrate.[4,7] The importance of charge transfer is further supported by experiments considering doping effects on bulk or multilayer FeSe.[12−16] These studies indicate that phonons and electrons from the substrate are key reasons for the boosted T_c in FeSe/STO.

In addition to the substrate effects mentioned above, the substrate also expands the lattice of the FeSe monolayer. Previous experiments suggested that a higher T_c could be achieved in heavily electron-doped FeSe compounds with a larger lattice constant[3] and hence linked the strain effect to iron-based superconductivity. The researchers then considered that if the lattice constant is a key factor for the enhancement of T_c, could T_c be further raised by increasing the lattice constant? Also, because of the lack of long-range magnetic order, the relationship among anti-ferro magnetism (AFM), nematicity and superconductivity in FeSe/STO is still ambiguous. What are the magnetic behaviors in monolayer FeSe, and how does lattice strain affect them? The answers to the above questions are critical for revealing the superconducting mechanism of iron-based superconductors.

In this Letter, we report the investigation of the magnetism of FeSe and FeTe monolayers with various lattice constants and electron doping. We find that tensile strain changes the magnetic phases from pair-checkerboard AFM (PAFM) to collinear AFM (CAFM) in an FeSe monolayer. Electron doping, on the other hand, will lower the difference of effective magnetic exchange parameters between the a and b directions and thus suppress the nematicity. We suggest that the effect of tensile strain and electron doping from an STO substrate suppresses both the nematic and magnetic orders of the FeSe monolayer, which is beneficial for the appearance of high-temperature superconductivity.

Our first-principles calculations employed the plane-wave basis and the projected augmented wave (PAW)[17,18] method encoded in the Vienna *ab initio* simulation package (VASP).[19,20] To study the FeSe and FeTe monolayers, we constructed a slab model which contains one layer of free-standing FeSe or FeTe, and over 20 Å vacuum layer was added to decouple the interlayer couplings for both materials. The PAW pseudopotential with the generalized gradient approximation of Perdew–Burke–Ernzerhof[21] for exchange-correlation potential was adopted in all calculations. A plane-wave cutoff energy of 450 eV was implemented. For structural relaxation, all the inner atomic positions were fully optimized and the atoms were allowed to relax until the atomic forces were smaller than 0.01 eV/Å. Here we used the small angle method[22] to extract the effective exchange parameters of relaxed FeSe and FeTe monolayer structures. We take into account the magnetic interac-

*Supported by the National Natural Science Foundation of China, the Special Funds for Major State Basic Research, the Qing Nian Ba Jian Program, and the Fok Ying Tung Education Foundation.

**Corresponding author. Email: xggong@fudan.edu.cn

© 2019 Chinese Physical Society and IOP Publishing Ltd

tions with the nearest, next-nearest, and next-next-nearest neighbor Heisenberg couplings J_1, J_2, and J_3, and the nearest-neighbor biquadratic interactions K_1. A supercell $(2\sqrt{2} \times 2\sqrt{2} \times 1)$ of 16 Fe atoms and a Monkhorst–Pack mesh of $4 \times 4 \times 1$ k points were used to calculate the effective exchange parameters of J_1, J_2, and K_1. A supercell $(2\sqrt{2} \times 4\sqrt{2} \times 1)$ contains 32 Fe atoms, and a Monkhorst–Pack mesh of $4 \times 2 \times 1$ k points was used for the calculation of J_3 for both FeSe and FeTe monolayers.

To investigate the magnetic properties of FeSe and FeTe monolayers, we considered three different AFM orders as shown in Fig. 1: CAFM (Fig. 1(a)), bi-collinear AFM (BCAFM) (Fig. 1(b)) and PAFM (Fig. 1(c)). The CAFM order is the magnetic ground state for the parent compounds of most iron-based superconductors.[23] The BCAFM order is a unique AFM pattern found in FeTe both experimentally and theoretically.[24,25] The PAFM order is the calculated magnetic ground state for both bulk and monolayer FeSe by first-principles calculations.[26] To start with, we performed total energy calculations for both the materials as a function of lattice constant ranging from 3.65 Å to 4.05 Å, which encompasses the lattice constants of bulk FeSe (3.765 Å), bulk FeTe (3.82 Å), and FeSe/STO (3.905 Å).

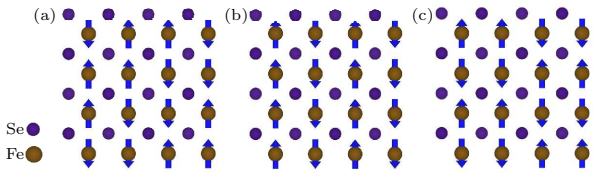

Fig. 1. Magnetic structures for FeSe and FeTe. Schematic diagrams of (a) the bi-collinear AFM order, (b) the collinear AFM order, and (c) the pair-checkerboard order.

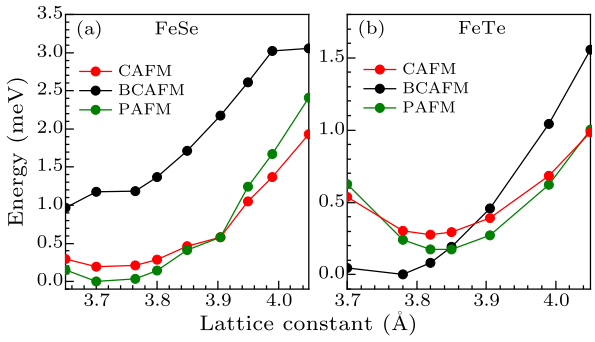

Fig. 2. Total energy versus lattice constant calculated for CAFM, BCAFM, and PAFM phases of (a) FeSe monolayer and (b) FeTe monolayer. The lowest energy states are PAFM and BCAFM for the FeSe monolayer at 3.765 Å and the FeTe monolayer at 3.82 Å, respectively.

The calculated total energies in Fig. 2 show that the lowest energy magnetic orders change as the lattice constant increases. As depicted in Fig. 2(a), the PAFM order is the lowest energy order for monolayer FeSe between 3.65 Å and 3.905 Å. The total energy of the PAFM order at 3.765 Å is 11 meV/Fe lower than that of the CAFM order, and 72 meV/Fe lower than that of the BCAFM order, respectively, which is in good agreement with the previous calculations.[26] The CAFM order turns out to be more stable than the PAFM order above about 3.905 Å, and the relative stability of the CAFM order over the PAFM order is further enhanced as the lattice constant further increases. However, for the FeTe monolayer, as shown in Fig. 2(b), the BCAFM order prevails over both the PAFM and CAFM orders below 3.85 Å. When the FeTe monolayer is further extended over 4.05 Å, the CAFM order replaces the PAFM order as the lowest energy order.

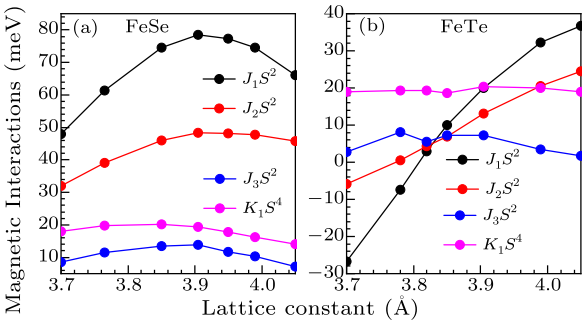

Fig. 3. The magnetic interactions J_1, J_2, J_3, and K_1 with varying lattice constants for (a) FeSe monolayer and (b) FeTe monolayer. The magnetic interactions show a parabolic shape with expanding lattice constant for the FeSe monolayer while they increase monotonically for the FeTe monolayer.

To quantify the magnetic interactions of FeSe and FeTe monolayers, we employed the model by adding the non-Heisenberg biquadratic interactions into the conventional Heisenberg model as proposed in Refs. [27,28]. We chose the PAFM order and BCAFM order to perform the small-angle method calculations for FeSe and FeTe monolayers, respectively. The magnetic interactions for FeSe and FeTe monolayers with varying lattice constants are shown in Fig. 3. For an FeSe monolayer, J_1 and J_2 exhibit a downward parabolic shape with the maximum around 3.905 Å, while for the FeTe monolayer, both J_1 and J_2 increase monotonically. This can be quantitatively understood by considering the height of Se/Te atoms with respect to the Fe plane and the distance between Fe and Se/Te atoms. As the lattice constant increases, the Se/Te atoms become closer to the Fe plane, and the Fe–Se–Fe angle approaches 180°, which enlarges the overlap between Se/Te p and Fe d orbitals, and the superexchange interactions become stronger. At the same time, the distance between Fe and Se/Te atoms increases, which weakens the related interactions. In this perspective, the two effects will compete with each other as the lattice constant increases and show dif-

ferent characteristics for FeSe and FeTe monolayers. The parameters K_1 and J_3 have relatively small values compared with J_1 and J_2 in an FeSe monolayer while possessing significant values for an FeTe monolayer. Instead of focusing on the specific magnitudes of J_s and K_s, we are more interested in understanding the magnetic behaviors of FeSe and FeTe monolayers in the context of the magnetic phase diagram, especially near the boundaries between different phases. Thus we take into account the analytical solutions for magnetic phase boundaries from the $J_1-J_2-J_3-K_1$ phase diagram:[28] $J_1 - 2J_3$ for the boundary between the BCAFM phase and PAFM phase (BCAFM/PAFM), and $J_1+2J_3-2J_2$ for the boundary between the PAFM phase and CAFM phase (PAFM/CAFM). The model also predicts the degeneracy of all the $q \sim (\pi, Q)$ AFM states at the PAFM/CAFM phase boundary.[28]

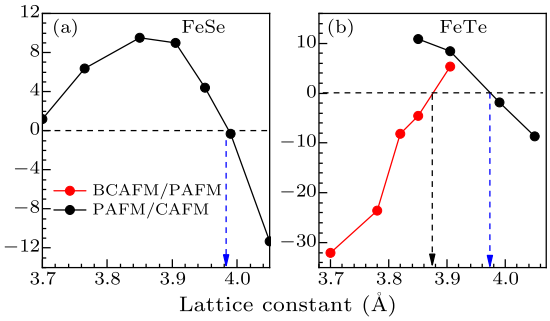

Fig. 4. Exchange parameters $J_1 - 2J_3$ (red dots) and $2J_3 + J_1 - 2J_2$ (black dots) versus lattice constant for (a) FeSe monolayer and (b) FeTe monolayer. The vertical dashed lines of $J_1 - 2J_3 = 0$ and $2J_3 + J_1 - 2J_2 = 0$ denote the critical lattice constant where BCAFM/PAFM and PAFM/CAFM phase transitions take place, respectively.

We found significant transitions between different phases induced by tensile strain in both FeSe and FeTe monolayers. As shown in Fig. 4, the black dots represent the distance to the PAFM/CAFM phase boundary and the red dots represent the distance to the BCAFM/PAFM phase boundary, respectively. For an FeSe monolayer, the black dots increase steadily as the lattice constant increases to 3.85 Å. This increment region means that the FeSe monolayer moves away from the PAFM/CAFM phase boundary and enhances PAFM as the magnetic ground state. These characteristics of magnetic interaction behavior are in accordance with the total energy calculations (Fig. 2(a)) below 3.70 Å. Above 3.85 Å, the decreasing values of the black dots show that the FeSe monolayer is approaching the PAFM/CAFM phase boundary. Around 3.98 Å, it hits the PAFM/CAFM phase boundary and the CAFM phase becomes more stable than the PAFM phase from this point on. This magnetic phase transition induced by strain itself is a prominent and significant phenomenon in the study of magnetism for FeSe/STO. Moreover, phase transitions are always accompanied by other intriguing physics; for instance, during the PAFM/CAFM phase transition, substantial spin fluctuations would emerge, especially those at $q \sim (\pi, 0)$, which are critical in inducing superconductivity in many other iron-based superconductors in the standard $S\pm$ pairing mechanism. For an FeTe monolayer, we found two such transitions. The values of the red dots in Fig. 4(b) increase monotonically from a large negative value to a positive value with increasing lattice constant. At around 3.97 Å, the FeTe monolayer experiences the second transition from the PAFM phase to the CAFM phase.

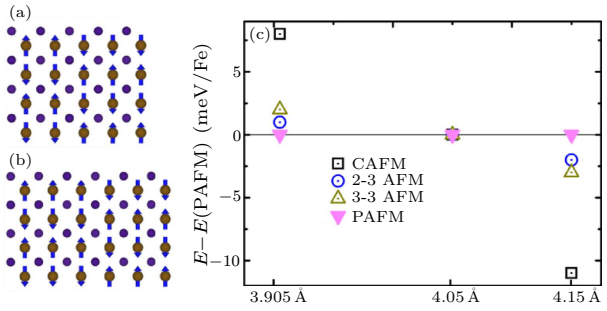

Fig. 5. (a) The 2–3 AFM configuration, (b) 3–3 AFM configuration, and (c) total energy of an FeTe monolayer adopting CAFM, 2–3 AFM, 3–3 AFM and PAFM states. The calculated energy of PAFM states is set to zero in each lattice constant.

We further clarify that the model description and total energy calculation are in good agreement in describing the magnetic behaviors around the PAFM/CAFM phase boundary. Here we take an FeTe monolayer as an example, and the total energy calculation shows the degeneracy of PAFM and CAFM states at 4.05 Å. If it is at the PAFM/CAFM phase boundary, the model gives the degeneracy of all the $q \sim (\pi, Q)$ states.[28] To clarify this, we chose two other states designated 2–3 AFM (Fig. 5(a)) and 3–3 AFM (Fig. 5(b)) as representative (π, Q) states and performed the total energy calculation at 3.905 Å, 4.05 Å, and 4.15 Å as shown in Fig. 5(c). We found that not only are PAFM and CAFM states degenerate at 4.05 Å, they are also essentially degenerate with 2–3 and 3–3 AFM states. At 3.905 Å, the PAFM state has the lowest total energy with 2–3 AFM and 3–3 AFM as close second and third, and CAFM has the highest energy. This is consistent with the model description of an FeTe monolayer on the PAFM side of the PAFM/CAFM phase boundary. When the FeTe monolayer is at 4.15 Å, the CAFM state becomes the lowest energy state, 3–3 AFM and 2–3 AFM come next, and the PAFM state has the highest energy, which means that the FeTe monolayer is on the CAFM side. Thus the total energy calculation of the four states reveals the mechanism of an FeTe monolayer crossing the PAFM/CAFM phase boundary, which agrees with the model description.

Nematicity would be enhanced while the formation of long-range magnetic order will be hindered around a PAFM/CAFM magnetic phase boundary. When FeSe and FeTe monolayers are near the PAFM/CAFM phase boundary, the $q \sim (\pi, Q)$ spin fluctuations will prevent the formation of long-range magnetic order.[28] Based on our previous calculation, the lattice constant of bulk FeSe and FeSe/STO are both close to the PAFM/CAFM phase boundary, thus the lack of long-range magnetic order in experiments can be qualitatively understood. More importantly, all $q \sim (\pi, Q)$ spin fluctuations break the same a–b symmetry and enhance the nematicity.[28] In this way, the applied tensile strain to the PAFM/CAFM phase boundary enhances the nematicity and suppresses AFM order.

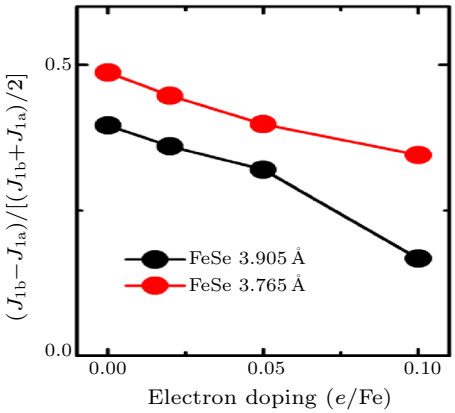

Fig. 6. The anisotropy of nearest-neighbor exchange parameter between the a and b directions with respect to electron doping.

However, we find that the electron doping will decrease the difference of the effective magnetic interaction between the a and b directions and hence suppress the nematicity. Just like in $CaFe_2As_2$,[29] where the difference of the nearest-neighbor exchange interaction reflects the broken symmetry between the a and b directions, here we perform the calculation of J_{1a} and J_{1b} to gain some understanding, where J_{1a} and J_{1b} represent the effective nearest neighbor exchange parameters along the a and b directions, respectively. In the PAFM phase, we have $J_{1a} = (J_{1F} + J_{1AF})/2$ and $J_{1b} = J_{1AF}$, where $J_{1F} = J_1 - 2KS^2$ and $J_{1AF} = J_1 + 2KS^2$ represent the ferro- and anti-ferro exchange parameter, respectively.[27] We also define the parameter $(J_{1b} - J_{1a})/[(J_{1b} + J_{1a})/2]$ to quantify the difference of the effective nearest-neighbor exchange parameter between the a and b directions. As shown in Fig. 6, the electron doping drives the effective exchange parameter along two directions closer, which is more obvious when the lattice constant is larger. Note that around the PAFM/CAFM phase boundary, spin fluctuations at $q \sim (\pi, Q)$ would choose the direction with the greater effect on J_1 as the anti-ferromagnetic direction. However, the approaching of J_{1a} and J_{1b} indicates that either the a or b direction could be chosen to be anti-ferromagnetically aligned. In this way, with substantial electron transfer from the substrate, the broken a–b symmetry induced by spin fluctuations at $q \sim (\pi, Q)$ will be compensated for and the nematicity will be suppressed.

Based on the above results, we can establish a relationship between the strain effect and superconductivity. The extended lattice of an FeSe monolayer to the PAFM/CAFM phase boundary prevents the appearance of long-range magnetic order and enhances the nematic order. The electron doping, on the other hand, decreases the nematicity. To sum up, with substantial electrons transferred from the substrate, the tensile strain to the PAFM/CAFM phase boundary will suppress the nematic order and long-range AFM order at the same time, which is the best condition for the rise of T_c. Experiments on iron-based superconductors show that there is a sharp shift of T_c when the Se/As height above the Fe plane approaches 1.37 Å.[30] Based on our calculation, the 1.37 Å height refers to the lattice constant of FeSe monolayers between 3.95 Å and 3.99 Å, which is around the PAFM/CAFM phase boundary, thus the strain effect and superconductivity are linked together again.

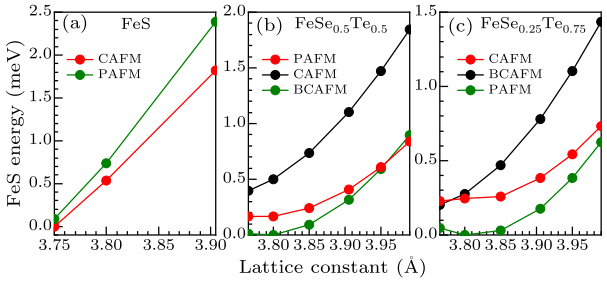

Fig. 7. Total energy versus lattice constant calculated for CAFM, BCAFM, and PAFM magnetic orders of (a) FeS monolayer, (b) $FeSe_{0.5}Te_{0.5}$ monolayer, and (c) $FeSe_{0.25}Te_{0.75}$ monolayer. All three iron chalcogenides show a tendency for a magnetic order transition from the PAFM order to the CAFM order.

Interestingly, we found that the transition from the PAFM phase to the CAFM phase can also be found in $FeSe_{0.5}Te_{0.5}$ with appropriate lattice strain. We performed the total energy calculation for three other iron chalcogenide monolayers: FeS, $FeSe_{0.5}Te_{0.5}$, and $FeSe_{0.25}Te_{0.75}$. As shown in Fig. 7, $FeSe_{0.5}Te_{0.5}$ shows signs of the lowest energy order transition from the PAFM state to the CAFM state. Based on the consistency between the total energy calculation and the model description as clarified before, we suggest that $FeSe_{0.5}Te_{0.5}$ could also reach the PAFM/CAFM phase boundary with proper tensile strain. The previous experiments found that one unit cell $FeSe_{0.4}Te_{0.6}$ exhibits a superconducting gap up to ~ 16.5 meV when grown on an STO substrate.[31] However, the lattice constant of $FeSe_{0.4}Te_{0.6}$/STO may still be a way from

the PAFM/CAFM phase boundary. We anticipate that the T_c of the $FeSe_{0.4}Te_{0.6}$ monolayer has a good potential to further increase with a larger lattice constant.

Finally, we suggested that one cannot further raise T_c of monolayer FeSe with a larger lattice constant than 3.98 Å. Peng *et al.* grew an FeSe monolayer on STO and BTO substrates with different lattice constants and found that, when expanding the lattice of FeSe/STO from 3.905 Å to around 3.98 Å, the gap-closing temperature increases from 65 K to around 70 K.[8] Based on our calculation, the FeSe monolayer is heading towards the PAFM/CAFM phase boundary in this region. With enough electrons transferred from the substrate, we expect an increasing T_c as the competing AFM and nematic order are suppressed. Larger lattice constants than 3.98 Å move the FeSe monolayer away from the PAFM/CAFM phase boundary, and the robust CAFM phase may finally prevent the emergence of superconductivity. However, the overall effect of strain in enhancing superconductivity may not be as profound compared with interfacial phonon or electron doping in FeSe/STO.

In conclusion, we have presented a first-principles calculation combined with a $J_1 - J_2 - J_3 - K_1$ model study of the magnetic interactions for FeSe and FeTe monolayers. It is found that the tensile strain induces the transition of magnetic phases. Electron doping will suppress the anisotropy of effective magnetic interaction between the a and b directions and hence the nematicity. Based on the above results, we suggest a close relationship between the strain effect and the underlying T_c of the monolayer FeSe high-temperature superconductor. Our work provides clues to understand the magnetic properties of the monolayer FeSe high-temperature superconductor and provides new insight into iron-based superconductivity.

References

[1] Wang Q Y et al 2012 *Chin. Phys. Lett.* **29** 037402
[2] Liu D et al 2012 *Nat. Commun.* **3** 931
[3] Tan S et al 2013 *Nat. Mater.* **12** 634
[4] He S et al 2013 *Nat. Mater.* **12** 605
[5] Lee J J et al 2014 *Nature* **515** 245
[6] Zhang W H et al 2014 *Chin. Phys. Lett.* **31** 017401
[7] Zhang W H et al 2014 *Phys. Rev. B* **89** 060506
[8] Peng R et al 2014 *Nat. Commun.* **5** 5044
[9] Rebec S N et al 2017 *Phys. Rev. Lett.* **118** 067002
[10] Lee D H 2015 *Chin. Phys. B* **24** 117405
[11] Rademaker L et al 2016 *New J. Phys.* **18** 022001
[12] Miyata Y et al 2015 *Nat. Mater.* **14** 775
[13] Wen C H P et al 2016 *Nat. Commun.* **7** 10840
[14] Lei B et al 2016 *Phys. Rev. Lett.* **116** 077002
[15] Shiogai J et al 2016 *Nat. Phys.* **12** 42
[16] Tang C et al 2016 *Phys. Rev. B* **93** 020507
[17] Blöchl P E 1994 *Phys. Rev. B* **50** 17953
[18] Kresse G and Joubert D 1999 *Phys. Rev. B* **59** 1758
[19] Kresse G and Furthmüller J 1996 *Comput. Mater. Sci.* **6** 15
[20] Kresse G and Furthmüller J 1996 *Phys. Rev. B* **54** 11169
[21] Perdew J P, Burke K and Ernzerhof M 1996 *Phys. Rev. Lett.* **77** 3865
[22] Zhu H F et al 2016 *Phys. Rev. B* **93** 024511
[23] Clarina de la C et al 2008 *Nature* **453** 899
[24] Bao W el at 2009 *Phys. Rev. Lett.* **102** 247001
[25] Li S L et al 2010 *Phys. Rev. Lett.* **105** 157002
[26] Cao H Y et al 2015 *Phys. Rev. B* **91** 020504
[27] Hu J P et al 2012 *Phys. Rev. B* **85** 144403
[28] Glasbrenner J K et al 2015 *Nat. Phys.* **11** 953
[29] Zhao J et al 2009 *Nat. Phys.* **5** 555
[30] Chen X H et al 2014 *Natl. Sci. Rev.* **1** 371
[31] Li F S et al 2015 *Phys. Rev. B* **91** 220503